# Refinement of the crystal structure of kanonaite, $(Mn^{3+},Al)^{[6]}(Al,Mn^{3+})^{[5]} O[SiO_4]$

ZDENĚK WEISS

*Coal Research Institute*
*71607 Ostrava-Radvanice, Czechoslovakia*

S. W. BAILEY

*Department of Geology and Geophysics*
*University of Wisconsin-Madison*
*Madison, Wisconsin 53706, U.S.A.*

AND MILAN RIEDER

*Institute of Geological Sciences, Charles University*
*12843 Praha 2, Czechoslovakia*

## Abstract

Kanonaite is orthorhombic and isotypic with andalusite. The space group is *Pnnm*; the cell data are $a = 7.959(2)$ Å, $b = 8.047(2)$ Å, $c = 5.616(1)$ Å. Refinement of 472 independent intensities yielded a distribution of manganese between a six-coordinated $M(1)$ ($Mn_{0.74} Al_{0.26}$) and a five-coordinated $M(2)$ ($Mn_{0.12}Al_{0.88}$) position. Mean interatomic distances are $M(1)-O = 2.003$ Å, $M(2)-O = 1.850$ Å, $Si-O = 1.630$ Å.

The Jahn–Teller bipyramidal distortion of $M(1)$ octahedra in kanonaite is surpassed by very few $Mn^{3+}$ octahedra in compounds whose structures have been refined. Si tetrahedra appear more regular in kanonaite than in andalusite and $M(2)$ polyhedra in both structures are about equally irregular.

Possessing analogously distorted Al(1) octahedra that share opposite short edges, andalusite displays features common to structures with oxygen-coordinated $Mn^{3+}$, and apparently invites relatively easy substitution in the andalusite–kanonaite series. Other evidence notwithstanding, the substitution is coupled with marked changes of intensities in the powder pattern.

## Introduction

Kanonaite ($Mn^{3+}_{0.76} Fe^{3+}_{0.02}Al_{1.23})SiO_5$, is a recently described mineral related to andalusite by the substitution $Al \rightleftharpoons Mn^{3+}$ (Vrána *et al.*, 1978). The composition of the original material is not that of an end member, the mole fraction of $Mn^{3+}AlSiO_5$ being 0.76. But the mineral is the richest in manganese of any of the natural or synthetic andalusite-type phases found or grown to date.

X-ray data indicated kanonaite to be isotypic with andalusite. Thus $Mn^{3+}$ and Al can enter the six-coordinated $M(1)$ and/or the five-coordinated $M(2)$ position. Vrána *et al.* (1978) assigned all manganese to the six-coordinated position, chiefly because the intensities measured on precession photographs compared favorably to those calculated for the structure of andalusite (Burnham and Buerger, 1961) with an appropriate quantity of $Mn^{3+}$ in octahedra; models with manganese distributed equally between six- and five-coordinated positions and with all manganese in five-fold coordination had to be rejected. Octahedral coordination of manganese was further supported by a subnormal magnetic moment (3.15 Bohr magnetons per one manganese atom) not explicable in terms of a five-fold coordination.

However, *some* manganese could reside in the five-coordinated position. To check this possibility and to study in detail the distortions of the coordination polyhedra, a structure refinement of the type material was essential.

## Experimental

The intensities were obtained on a Syntex P2$_1$ diffractometer in the $\theta$:2$\theta$ variable scan mode using graphite-monochromatized Mo$K\alpha$ radiation. A standard reflection was monitored after every fifty reflections to check crystal and electronic stability. Reflections were considered as observed if I > 3$\sigma$(I), where I = [S – (B$_1$ + B$_2$)/B$_r$]T$_r$, S being the scan count, B$_1$ and B$_2$ the background, B$_r$ the ratio of background time to scan time, and T$_r$ the 2$\theta$ scan ratio in degrees per minute. $\sigma$(I) was calculated from standard counting statistics.

All reflections out to 2$\theta$ = 60° in all eight octants were recorded. After being corrected for Lp and absorption (empirically by the psi-scan technique), the data were merged into a single octant. Thus each F value for a general reflection is an average of eight measurements. The merging program automatically rejects reflections with individual F values after correction that do not agree with one another, usually only true for the weakest reflections. It also rejects individual measurements that deviate by more than 2.5 standard deviations from the average of the other equivalent reflections. In all, there were 4,223 actual measurements yielding 472 independent observed values. The few rejections made (95 out of 4,223) indicate that the data set is a very good one. The merging process assumed orthorhombic symmetry established by the precession method, but assumed no systematic absences; the symmetry is confirmed by the low number of rejections and no violations of systematic absences.

Least-squares refinement of 15 reflections (2$\theta$ between 39.8° and 50.4°) gave the following orthorhombic cell, $a$ = 7.959(2)Å, $b$ = 8.047(2)Å, $c$ = 5.616(1)Å. Interaxial angles were within 0.03° of 90°, with standard errors of 0.02°.

Computer programs employed include FOBS and SORTMERGE for data reduction (University of Wisconsin), FOUR for electron density calculations (Weiss, unpublished), ORFLS (Busing et al., 1962) as modified by Ďurovič for refining the distribution of elements competing for several positions, and programs DIST and DIFZ for interatomic distances and bond angles and for theoretical powder patterns (Weiss and Krajíček, 1979).

## Refinement and results

The anticipated structure was checked by several electron density sections and difference maps. Both the precession and diffractometer intensities clearly showed that the structure is very close to that of andalusite.

In the refinement, which was performed in space group *Pnnm*, two simplifying assumptions were made: first, all atoms were treated as neutral and corresponding scattering factors were used (Cromer and Waber, 1965) and, second, only Mn and Al were assumed to populate six- and five-coordinated positions. The trace of Fe was ignored. Only diffractometer intensities were used, and three structural models were tested initially: (1) all manganese in position $M$(1), (2) 95% of all manganese in $M$(1), and (3) 60% of all manganese in $M$(1). Models (1) and (3) did not converge; what follows concerns model (2) only. The refinement proceeded in several steps, each of which involved a number of cycles (iterations). Generally, the results of previous steps were not varied in the following ones.

The first step was scaling of the data (unweighted $R_1$ = 16.4%). Next, atomic coordinates were included assuming the distribution of Mn between $M$(1) and $M$(2) to be that of model (2). The corresponding $R_1$ was 7.3% and dropped to 6.1% as Mn was allowed to redistribute between $M$(1) and $M$(2). The inclusion of isotropic temperature factors for cations and anisotropic for oxygen produced an $R_1$ = 4.1%. In the final step, which included anisotropic temperature factors for all atoms and in which all parameters were varied simultaneously, $R_1$ settled down at 3.1% (unweighted) and 4.5% (weighted).

Final atomic coordinates and temperature factors are summarized in Table 1, the most important interatomic distances and angles in Table 2. A list of F(obs.) and F(calc.) appears in Table 3.[1] Like that of andalusite, the structure of kanonaite is composed of three types of polyhedra with six-, five-, and fourfold coordination, respectively. Octahedra around the $M$(1) cations share opposite edges ("*trans*") and make up ribbons running parallel to [001], with the $M$(1) cations on a common twofold axis, Chains composed of alternating polyhedra around $M$(2) and Si are parallel to [001] also; the polyhedra share corners with one another and with octahedra in the ribbons. Adjacent $M$(2)–Si chains are connected by an edge common to two $M$(2) polyhedra. The chief building units are illustrated in Figure 1. Being the

---

Table 1. Atomic coordinates and temperature factors for kanonaite, space group *Pnnm*

| Atom | $Mn_{0.74}Al_{0.26}$ | $Mn_{0.12}Al_{0.88}$ | Si | O | O | O | O |
|---|---|---|---|---|---|---|---|
| Position * | M(1), $e$ | M(2), $g$ | $g$ | O(1), $g$ | O(2), $g$ | O(3), $g$ | O(4), $h$ |
| Point symmetry | 2 | $m$ | $m$ | $m$ | $m$ | $m$ | 1 |
| $x$ | 0 | -0.1252(2) ** | 0.2494(2) | 0.0743(4) | 0.4243(3) | 0.1042(3) | 0.2430(3) |
| $y$ | 0 | 0.3630(2) | 0.2549(2) | -0.1369(4) | 0.3626(3) | 0.3989(3) | 0.1413(3) |
| $z$ | 0.2429(1) | 0 | 0 | 0 | 0 | 0 | 0.2383(3) |
| $\beta_{11}$ | 33(1) *** | 36(1) | 25(1) | 39(3) | 31(3) | 25(3) | 44(2) |
| $\beta_{22}$ | 25(1) | 37(1) | 21(1) | 29(3) | 38(3) | 24(3) | 35(2) |
| $\beta_{33}$ | 55(2) | 84(3) | 55(3) | 68(7) | 75(7) | 99(7) | 72(5) |
| $\beta_{12}$ | 5(1) | -1(1) | 3(1) | 1(3) | 1(3) | 1(2) | 1(2) |
| $\beta_{13}$ | 0 | 0 | 0 | 0 | 0 | 0 | -6(2) |
| $\beta_{23}$ | 0 | 0 | 0 | 0 | 0 | 0 | 6(3) |
| Equivalent $B(\AA^2)$ | 0.714 | 0.975 | 0.617 | 0.860 | 0.901 | 0.789 | 0.963 |

*Multiplicity for positions e and g is 4, h has a multiplicity of 8.*
**Errors are given in units of the last digit.*
***Coefficients of anisotropic temperature factors were multiplied by $10^4$.*

same as in andalusite, the arrangement of polyhedra in kanonaite can be visualized from drawings in Burnham and Buerger's (1961) paper.

The differences between kanonaite and andalusite are localized at the sites of the trivalent manganese. The refined occupancies are $Mn_{0.74}Al_{0.26}$ for $M(1)$ and $Mn_{0.12}Al_{0.88}$ for $M(2)$, yielding a bulk composition of $Mn_{0.86}Al_{1.14}$, The chemically obtained composition is $Mn_{0.76}^{3+}Fe_{0.02}^{3+}Al_{1.23}$. The crystal X-rayed has not been analyzed, but the data of Vrána *et al.* (1978) show that chemical heterogeneity alone is an unlikely cause of the difference; hence, simplifications made during the refinement must have contributed. From the results of the refinement it is apparent that when opting for all manganese in sixfold coordination, Vrána *et al.* (1978) came close to the real distribution. In fact, the same distribution was assumed by Abs-Wurmbach *et al.* (1981) who refined four structures on the andalusite–kanonaite join (including kanonaite), although Mössbauer spectra indicated that 10 to 15% of total iron resides in $M(2)$.

Even though manganese is not the sole occupant of $M(1)$ octahedra, it must have been instrumental in distorting them to elongated quasi-bipyramids, typical of the high-spin $d^4$ Jahn–Teller configuration. This is illustrated in Figure 2 showing the relation between mean bond length, $\bar{R}$, and distortion, $\Delta$. The plot represents most structures with oxygen-coordi-

Table 2. Bond lengths (Å units) and bond angles for kanonaite and andalusite

| | | Kanonaite | | Andalusite* | |
|---|---|---|---|---|---|
| 2x | M(1) – O(1) | 1.850(1) ** | | 1.829(4) | |
| 2x | M(1) – O(2) | 1.916(1) | | 1.892(4) | |
| 2x | M(1) – O(4) | 2.242(3) | | 2.085(3) | |
| 2x | O(1) – O(2) | 2.810(2) | 96.5(1)° | 2.780(1) | 96.7(2)° |
| | O(1) – O(1)' | 2.498(3) | 84.9(1)° | 2.476(7) | 85.2(3)° |
| | O(2) – O(2)' | 2.516(3) | 82.1(1)° | 2.469(7) | 81.5(3)° |
| 2x | O(1)' – O(4) | 2.932(5) | 91.0(2)° | 2.793(6) | 90.8(3)° |
| 2x | O(1) – O(4) | 2.857(4) | 88.0(2)° | 2.738(6) | 88.5(3)° |
| 2x | O(2)' – O(4) | 2.992(5) | 91.7(2)° | 2.854(6) | 91.6(3)° |
| 2x | O(2) – O(4) | 2.931(5) | 89.3(2)° | 2.794(6) | 89.1(3)° |
| | M(2) – O(1)'' | 1.862(5) | | 1.816(6) | |
| | M(2) – O(3) | 1.847(3) | | 1.843(5) | |
| | M(2) – O(3)' | 1.921(3) | | 1.886(6) | |
| 2x | M(2) – O(4) | 1.806(4) | | 1.818(3) | |
| | O(4) – O(4)'' | 2.941(4) | 109.0(3)° | 2.901(4) | 105.9(3)° |
| 2x | O(4) – O(3) | 3.245(5) | 125.3(5)° | 3.265(7) | 126.2(6)° |
| 2x | O(4) – O(3)' | 2.727(2) | 94.0(2)° | 2.677(5) | 92.5(3)° |
| 2x | O(4) – O(1)'' | 2.730(5) | 96.2(3)° | 2.761(5) | 98.9(3)° |
| | O(3) – O(3)' | 2.321(4) | 76.0(2)° | 2.247(7) | 74.1(3)° |
| | O(3) – O(1)'' | 2.540(2) | 86.4(2)° | 2.515(7) | 86.8(4)° |
| 2x | Si – O(4) | 1.622(4) | | 1.631(4) | |
| | Si – O(2)'' | 1.638(4) | | 1.635(5) | |
| | Si – O(3)'' | 1.635(2) | | 1.615(6) | |
| | O(4) – O(4)'' | 2.678(3) | 111.3(3)° | 2.658(4) | 109.1(4)° |
| 2x | O(3)'' – O(4) | 2.702(3) | 112.1(3)° | 2.681(6) | 111.4(5)° |
| 2x | O(2)'' – O(4) | 2.653(5) | 108.9(4)° | 2.703(5) | 111.7(5)° |
| | O(2)'' – O(3)'' | 2.562(5) | 103.0(3)° | 2.514(7) | 101.3(5)° |

* The lengths are those of Burnham and Buerger /1961/, slightly corrected; angles were calculated.
** Errors are given in units of the last digit and reflect errors of atomic coordinates, not those of the unit cell.
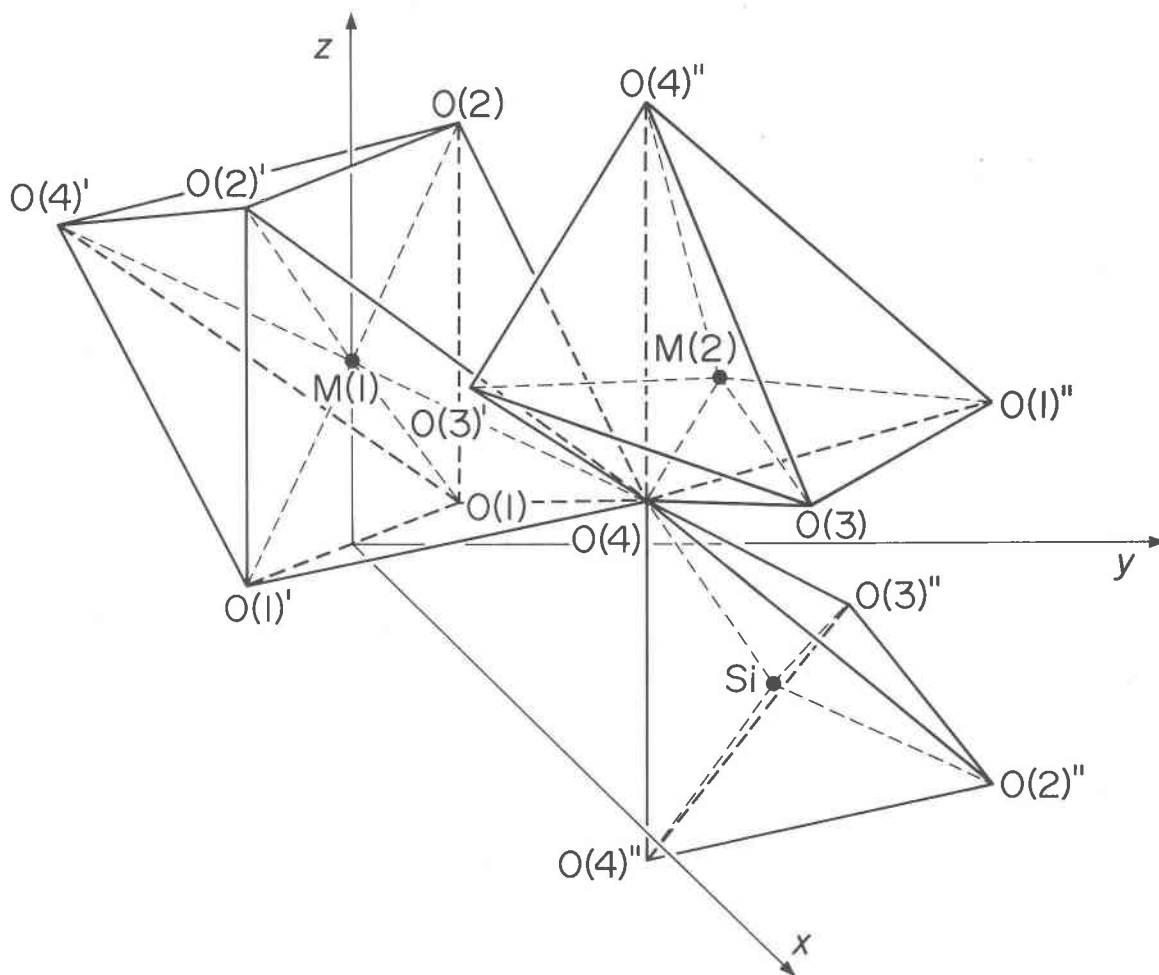
Fig. 1. A perspective drawing of the three coordination polyhedra in the structure of kanonaite.

nated $Mn^{3+}$ refined to date. (Due to their low precision, data for hausmannite (Satomi, 1961) and flinkite (Moore, 1967) defy a meaningful interpretation and are not shown.) The $\bar{R}$ of kanonaite (2.003Å) is obviously lowered by aluminum and cannot be plotted. However, its octahedral distortion is the third highest on record among octahedra occupied by $Mn^{3+}$ alone. It has been argued (Shannon *et al.,* 1975) that positive deviations from the trend in Figure 2 reveal the presence of some divalent manganese on the position, which appears to be the case for Mn(3) in pinakiolite (Moore and Araki, 1974). The same might be at work for $M(1)$ and $M(2)$ of orthopinakiolite (Takéuchi *et al.,* 1978) refined later. The corresponding points (O, P in Fig. 2) were not included in the regression. If this is a valid argument and if it is legitimate to correct $\bar{R}$ of $M(1)$ in kanonaite linearly for the proportion of aluminum by using $\bar{R}$ of Al(1) in andalusite, the point plots some-

what below the regression line ($\bar{R}$(corr.) = 2.027Å), ruling out a $Mn^{2+}$ content due to a conceivable substitution of $Mn^{2+}AlSiO_4(OH)$.

It should be noted that there are interesting analogies between kanonaite and other phases with $Mn^{3+}$. The ribbon-like arrangement of *trans*-edge-sharing octahedra whose longest bonds are perpendicular to the axis of the ribbon dominates the structures of groutite (Dent Glasser and Ingram, 1968), manganite (Dachs, 1963), and pinakiolite (Moore and Araki, 1974), and it is present in orthopinakiolite (Takéuchi *et al.,* 1978) and hausmannite (Satomi, 1961). The same holds for bermanite except that it is a pair of *shorter bonds* that are perpendicular to the ribbon (Kampf and Moore, 1976). Admittedly, three of the six neighboring oxygens in groutite and manganite belong to OH groups, thus imposing another kind of influence on the octahedra. Also, the complex edge sharing in orthopinakiolite and hausmannite con-
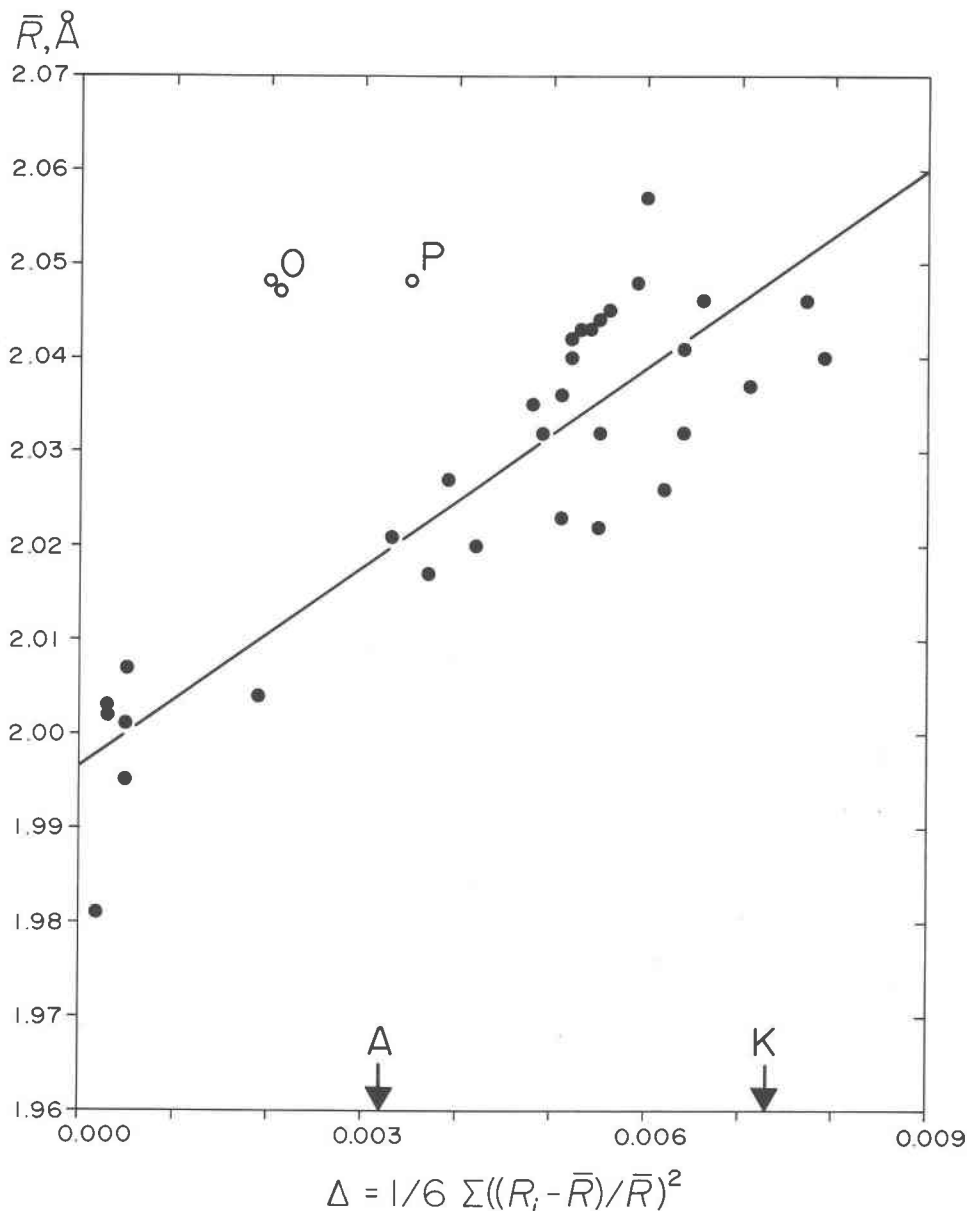
Fig. 2. A plot of mean $Mn^{3+}$–O distance ($\bar{R}$) vs. octahedral distortion ($\Delta$). The data used by Shannon et al. (1975) were supplemented with data for $\alpha$-$Mn_2O_3$ (Geller, 1971), braunite (de Villiers, 1975; Moore and Araki, 1976), bermanite (Kampf and Moore, 1976), orthopinakiolite (Takéuchi et al., 1978), and CMS-XI (Moore and Araki, 1979); average esd's were omitted. Three points (open circles, see text) were left out when calculating the regression line $\bar{R} = 7.0495 + 1.9965$. Arrows mark distortions of $M(1)$ octahedra in kanonaite (K) and andalusite (A).

strains the ribbon geometry. If this argument is as favorable as it appears to be, however, it is little wonder that andalusite, which has the same arrangement of aluminum-occupied $M(1)$ octahedra, readily allows substitution of $Mn^{3+}$. The substitution of $Mn^{3+}$ is further facilitated owing to a distortion of $M(1)$ octahedra resembling the Jahn–Teller effect even in Mn-free specimens, although aluminum does not have the electron configuration to produce a true Jahn–Teller effect. In fact, the distortion $\Delta$ for $M(1)$ occupied by aluminum alone is larger than that measured in a number of octahedra around trivalent manganese (Fig. 2).

Effective coordination numbers and mean effective ionic radii (Hoppe, 1979) were calculated to compare coordination in kanonaite and andalusite (Table 4).

Table 4.  Mean fictive ionic radii and effective coordination
numbers for kanonaite and andalusite

| Atom | Starting ionic radius (Å) | Mean fictive ionic radius $^1$MEFIR (Å) * | | Effective coordination number $^1$ECoN ** | |
|------|------|------|------|------|------|
|      |      | Kanonaite | Andalusite | Kanonaite | Andalusite |
| M(1) | 0.53 | 0.56 | 0.52 | 4.6  | 5.3  |
| M(2) | 0.48 | 0.47 | 0.47 | 4.9  | 5.0  |
| Si   | 0.26 | 0.26 | 0.25 | 4.0  | 4.0  |
| O(1) | 1.40 | –    | –    | 11.2 | 11.9 |
| O(2) | 1.40 | –    | –    | 11.0 | 11.5 |
| O(3) | 1.40 | –    | –    | 7.7  | 6.8  |
| O(4) | 1.40 | –    | –    | 11.9 | 12.7 |

\*  $^1$MEFIR *values for oxygen atoms were not calculated.*
\*\* $^1$ECoN *values include all surrounding atoms.*

The effective coordination numbers for $M(1)$ and $M(2)$ in kanonaite are lower than those in andalusite and equal for tetrahedra in both structures. The $^1$ECoN for $M(1)$ in kanonaite is even lower than for $M(2)$, pointing to a severe distortion of $M(1)$ octahedra. Inasmuch as the ECoN values reflect just the scatter of bond lengths between the central atom and the surrounding ones, we also considered the relative scatter of oxygen–oxygen bond lengths. In kanonaite the oxygen–oxygen bond lengths are less uniform for $M(1)$, but more uniform for $M(2)$ and markedly more so for Si, than their counterparts in andalusite. Considering all aspects, the $M(1)$ polyhedra are more distorted in kanonaite than in andalusite, but kanonaite's tetrahedra are more regular. The $M(2)$ polyhedra are about equally irregular in both structures.

The substitution of $Mn^{3+}$ in andalusite is coupled with a pronounced change in optical data (Vrána *et al.*, 1978) and cell parameters (Abs-Wurmbach *et al.*, 1981). The large differences between scattering factors for aluminum and manganese predict significant changes of the intensities of many reflections in powder patterns (Fig. 3), which may thus serve as a relatively simple check for the substitution.
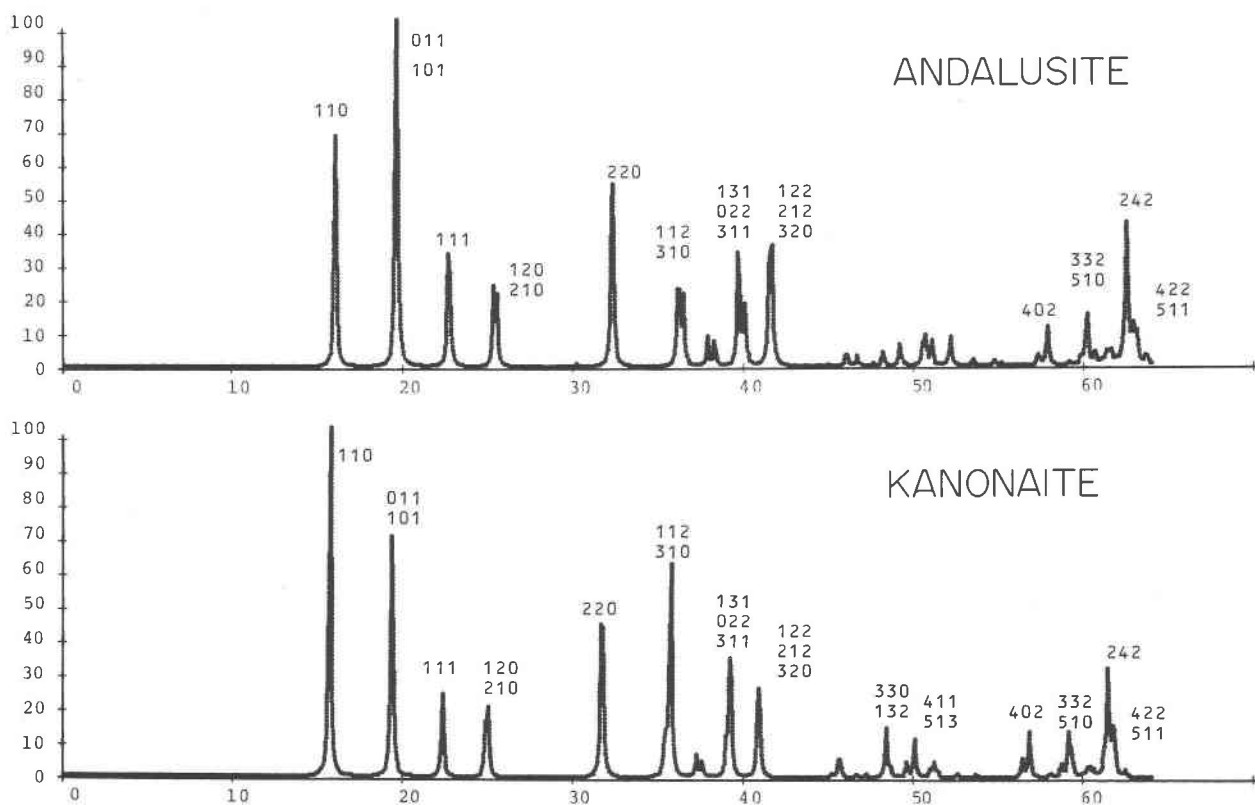
## Acknowledgments

Fig. 3. Diffractometer patterns of andalusite and kanonaite calculated with the DIFZ program. Monochromatic copper $K\alpha_1$ radiation ($2\theta$), intensities normalized to 100. Only the main *hkl* indices are shown, for complete indexing see Borg and Smith (1969) and Vrána *et al.* (1978).

# References

Abs-Wurmbach, I., Langer, K., Seifert, F., and Tillmanns, E. (1981) The crystal chemistry of $(Mn^{3+}, Fe^{3+})$—substituted andalusites (viridines and kanonaite), $(Al_{1-x-y}Mn_x^{3+}Fe_y^{3+})_2$ $(O|SiO_4)$: crystal structure refinements, Mössbauer, and polarized optical absorption spectra. Zeitschrift für Kristallographie, 155, 81–113.

Borg, I. Y. and Smith, D. K. (1969) Calculated X-ray powder patterns for silicate minerals. Geological Society of America Memoir 122.

Burnham, C. W. and Buerger, M. J. (1961) Refinement of the crystal structure of andalusite. Zeitschrift für Kristallographie, 115, 269–290.

Busing, W. R., Martin, K. O., and Levy, H. A. (1962) ORFLS, a Fortran crystallographic least-squares refinement program. U.S. National Technical Information Service, ORNL–TM–305.

Cromer, D. T. and Waber, J. T. (1965) Scattering factors computed from relativistic Dirac-Slater wave functions. Acta Crystallographica, 18, 104–109.

Dachs, H. (1963) Neutronen- und Röntgenuntersuchungen am Manganit, MnOOH. Zeitschrift für Kristallographie, 118, 303–326.

Dent Glasser, L. S. and Ingram, L. (1968) Refinement of the crystal structure of groutite, $\alpha$-MnOOH. Acta Crystallographica, B24, 1233–1236.

Geller, S. (1971) Structures of $\alpha$-$Mn_2O_3$, $(Mn_{0.983}Fe_{0.017})_2O_3$ and $(Mn_{0.37}Fe_{0.63})_2O_3$ and relation to magnetic ordering. Acta Crystallographica, B27, 821–828.

Hoppe, R. (1979) Effective coordination numbers (ECoN) and mean fictive ionic radii (MEFIR). Zeitschrift für Kristallographie, 150, 23–52.

Kampf, A. R. and Moore, P. B. (1976) The crystal structure of bermanite, a hydrated manganese phosphate. American Mineralogist, 61, 1241–1248.

Moore, P. B. (1967) Crystal chemistry of the basic manganese arsenate minerals 1. The crystal structures of flinkite,

$Mn_2^{2+}Mn^{3+}(OH)_4(AsO_4)$ and retzian, $Mn_2^{2+}Y^{3+}(OH)_4(AsO_4)$. American Mineralogist, 52, 1603–1613.

Moore, P. B. and Araki, T. (1974) Pinakiolite, $Mg_2Mn^{3+}O_2[BO_3]$; warwickite, $Mg(Mg_{0.5}Ti_{0.5})O[BO_3]$; wightmanite, $Mg_5(O)$ $(OH)_5[BO_3] \cdot nH_2O$: Crystal chemistry of complex 3Å wallpaper structures. American Mineralogist, 59, 985–1004.

Moore, P. B. and Araki, T. (1976) Braunite: its structure and relationship to bixbyite, and some insights on the genealogy of fluorite derivative structures. American Mineralogist, 61, 1226–1240.

Moore, P. B. and Araki, T. (1979) Crystal structure of synthetic $Ca_3Mn_2^{3+}O_2[Si_4O_{12}]$. Zeitschrift für Kristallographie, 150, 287–297.

Satomi, K. (1961) Oxygen positional parameters of tetragonal $Mn_3O_4$. Journal of the Physical Society of Japan, 16, 258–266.

Shannon, R. D., Gumerman, P. S., and Chenavas, J. (1975) Effect of octahedral distortion on mean $Mn^{3+}$–O distances. American Mineralogist, 60, 714–716.

Takéuchi, Y., Haga, N., Kato, T., and Miura, Y. (1978) Orthopinakiolite, $Me_{2.95}O_2[BO_3]$: its crystal structure and relationship to pinakiolite, $Me_{2.90}O_2[BO_3]$. Canadian Mineralogist, 16, 475–485.

de Villiers, J. P. R. (1975) The crystal structure of braunite with reference to its solid-solution behavior. American Mineralogist, 60, 1098–1104.

Vrána, S., Rieder, M., and Podlaha, J. (1978) Kanonaite, $(Mn_{0.76}^{3+}Al_{0.23}Fe_{0.02}^{3+})^{[6]}Al^{[5]}[O|SiO_4]$, a new mineral isotypic with andalusite. Contributions to Mineralogy and Petrology, 66, 325–332.

Weiss, Z. and Krajíček, J. (1979) Modeling of X-ray diffraction patterns. (in Czech) Vědeckovýzkumný uhelný ústav Ostrava, Samostatná publikace č.4.